M. WÓJCIK [1*]

HYBRID, MULTISCALE NUMERICAL SIMULATIONS OF THE EQUAL CHANNEL ANGULAR PRESSING (ECAP) USING THE CRYSTAL PLASTICITY THEORY

The FEM simulations of the ECAP including real conditions of the process – the friction between the metal extruded and the die walls, as well as, the channels rounding, were done here in two scales – macro- and micro-. The macroscopic analyses were done for isotopic material with a non-linear hardening using the UMAT user material procedure. The pure Lagrangian approach was applied here. The stress, strains and their increments, as well as, the deformation gradient tensor were recorded for selected finite elements in each calculation step. The displacements obtained in the macroscopic FEM analysis are then used as the kinematic input for the polycrystalline structure. The dislocation slip was included as the source of the plastic deformation here for the face-centered cubic structure. The results obtained with the use of the crystal plasticity show the heterogeneous distribution of stress and strain within the material associated with the grains anisotropy. The results in both micro- and macro- scales are coincident. The FEM analyses show the potential of the application of the crystal plasticity approach for solving elastic-plastic problems including the material forming processes.

Keywords: Crystal plasticity; ECAP process; CPFEM; polycrystals; crystalline structure

1. Introduction

The macroscopic solution of elastic-plastic analyses caused by the loading applied gives only the overall description of the problem restricted to the change of the body shape and the macroscopic distribution of stress and strain in a material. The crystal plasticity (CP) modelling is a powerful tool for prediction the microstructural changes in the material under loading, including the grain anisotropy, strain hardening, effect of grain size and the microstructure evolution, therefore. Such approach includes not only the change of the material shape, but also consists of the information about the mechanisms of the plastic deformation – i.e. dislocation slip, twinning, martensitic transformation and displacement of mobile phase boundaries. The CP theory coupled with the finite element method (CPFEM) is used to connect the macro- and micro- or even nano- scales to examine the deformation mechanisms of crystals, texture evolution, as well as, stress and strains distribution in the material at the level of a single grain.

The CP theory is useful in numerical analyses of Severe Plastic Deformation (SPD) methods giving the information not only about the deformation of the material, but also enables to evaluate the change of its microstructure. Among SPD processes which results in the high plastic deformation of the material and the refinement of grains to even nanoscale, the high-pressure torsion (HPT), multi-directional forging (MDF), the KOBO extrusion (the name of the method is composed of the first two letters of the surnames of Polish professors and inventors: A. Korbel and W. Bochniak), the friction stir processing (FSP) and the equal-channel angular pressing (ECAP or ECAE) are the most popular. Numerical simulations of SPD processes give the information about the material deformation [1], as well as, they enable to evaluate its microstructure. There are many publications considering the texture evolution during the SPD processes. In [2], the modelling of a texture evolution in the KOBO extrusion is presented. The study of plastic deformation behavior during high pressure torsion process by crystal plasticity finite element simulation (CPFEM) is contained in [3]. The modelling of the FSP in terms of the change of the microstructure is shown in [4].

The ECAP process is considered in this work. It is a discontinuous process which relies on a single or a multiple material extrusion through the angle channel with a constant cross-section (Fig. 1) [5]. The ECAP is characterized by the very high shear stresses and the accumulation of a very large plastic strains (even >300%) in the material which results in its microstructure

[1] RZESZOW UNIVERSITY OF TECHNOLOGY, FACULTY OF MECHANICAL ENGINEERING AND AERONAUTICS, DEPARTMENT OF MATERIALS FORMING AND PROCESSING, 8 POWSTAŃCÓW WARSZAWY AV., 35-959 RZESZÓW, POLAND

* Corresponding author: m.wojcik@prz.edu.pl

refinement to the ultra-fine sizes. Such reduction of grains size depends on the channel angle, number of ECAP passes, the extrusion speed, temperature, etc. [6-9]. According to Sadawy et al. [10], the grain size is reduced from 390 μm to even 0.3 μm after the ECAP method with 10 passes. The ultra-fine microstructure with a grain size at the range of 300-600 nm is obtained in the ECAP process in [11]. The effective plastic strain might be described as follows (Eq. 1) [12]:

$$\varepsilon_N = \frac{N}{\sqrt{3}}\left[2\cot\left(\frac{\varphi}{2}+\frac{\psi}{2}\right)+\psi\csc\left(\frac{\varphi}{2}+\frac{\psi}{2}\right)\right] \qquad (1)$$

where ε_N is the accumulated equivalent plastic strain in the ECAP, N is the number of passes, φ is the die channel angle, ψ is the outer corner angle, cot is the cotangents function and cosec is the cosecant one. In [12], the average effective plastic strain in a material is up to 260% after the ECAP process with two passes. In other work [13], the effective plastic strain up to 600% was obtained in the ECAP with one pass at 150°C temperature for an AA2011 aluminum alloy.
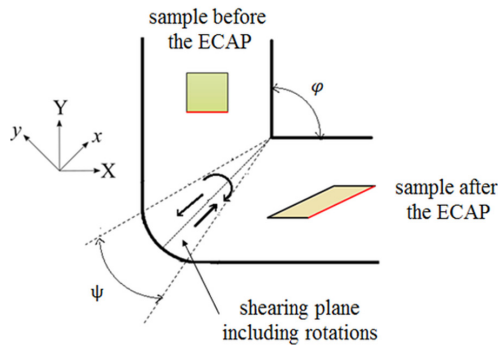

Fig. 1. The scheme of the ECAP process

The deformation in the ECAP process in the inner core is a simple shear occurring in the deformation zone in conjunction with the rotation. The cross-section of the material sample does not change during the process. The shear plane is rotated towards the extrusion direction by an angle equals the half of the channel bending (φ). The deformation state indicates on the tension in the x direction and on the compression in the y one, assuming also the rigid body rotation usually clockwise.

The simplified theoretical analysis based on the simple shear model is applied in modelling of the ECAP process. It assumes that the material is subjected to the simple shear at the intersection of two channels which cross at an angle 90°, resulting the concentration of a shearing in a small area and causes the large rotations. Real numerical simulations assuming real process conditions and the geometry of channels are also used. The FEM methods using the user material procedure enable to obtain information about the stress state and the deformation gradient in each calculation step. This data might be then used in microstructural analyses based on the crystal plasticity theory.

The numerical simulations of the ECAP require the selection of the proper crystal plasticity model which takes into account crystallographic anisotropy of grains and the texture

evolution in modelling of the mechanical behaviour of polycrystalline materials caused by the plastic deformation mechanisms, i.e. slip or twinning. The simple shear along the shear plane is the most frequently model to show the deformation during the ECAP. Nevertheless, it is only suitable for ideal conditions without friction, die with sharp angles and for a perfect plastic material. The application of a simple shear model in numerical modelling of the ECAP is presented in [14-16]. The Taylor model is a fully-constrained one in which it is assumed that each grain is subjected to the same plastic strain as the macroscopic one [17]. Five components of the plastic strain increment and five independent slip systems are necessary [18]. Although the strain uniformity fulfills the compatibility condition but not the equilibrium one at grain boundaries [19]. The examples of the use of the Taylor model in numerical analyses of the ECAP are described in [20-23]. The self-consistent model, in which each grain is assumed as a single ellipsoidal inclusion in a homogeneous equivalent medium, is developed in order to overcome limitations above [24]. In this approach, each grain of the polycrystalline material can deform differently depending on its directional properties [25]. The use of the self-consistent model in the modelling of the ECAP process is described in [26-29].

The numerical simulations in a macroscopic scale and based on the CP theory for the ECAP process assuming the dislocation slip as a main mechanism of a plastic deformation, are considered in this paper. The real conditions of the process – the friction between the metal extruded and the die walls, as well as, the channels rounding, were taken into account here. The macroscopic analysis was done using the pure Lagrangian approach and the UMAT user material procedure. The displacements obtained in the macroscopic FEM analysis are the kinematic input for the polycrystalline structure. The stress and plastic strain distributions, as well as, the pole figures in the polycrystalline material after the ECAP with one pass were analyzed. The main advantage of the approach based on the CP theory is that it includes not only the macroscopic behaviour of a material under loading but also gives information about the plastic deformation of a single grain in a polycrystal.

2. Kinematical equations of the CP theory

The kinematical theory applied in the CPFEM model is based on the approach proposed by Asaro [30] and Asaro and Needleman [31]. Three configurations are considered here. The initial configuration corresponds to the undeformed state of the material and the current configuration indicates the deformed one. The intermediate configuration obtained from the current configuration describes the rotation and stretching (Fig. 2). Therefore, the deformation gradient tensor might be decomposed multiplied as follows (Eq. 2):

$$\boldsymbol{F} = \boldsymbol{F}^* \cdot \boldsymbol{F}^p \qquad (2)$$

where $\boldsymbol{F}$ is the total deformation gradient tensor, $\boldsymbol{F}^*$ is a part of the total deformation gradient tensor which is responsible for

the stretching and the rotation of the lattice structure and F^p indicates the plastic shearing on selected crystalline slip planes.
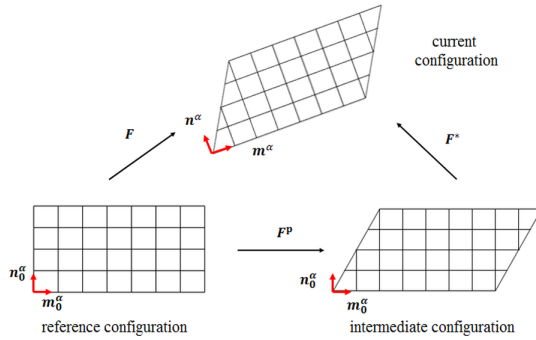

Fig. 2. Multiplicative decomposition of the deformation gradient into elastic and plastic deformation parts

Based on the tensor F, the velocity gradient one (L) can be determined in line with Eq. (3) and further, might be decomposed additively into both elastic and plastic parts (Eq. 4) and into symmetric and antisymmetric ones (Eq. 5):

$$L = \dot{F} F^{-1} \tag{3}$$

$$L = L^e + L^p \tag{4}$$

$$L = \dot{\varepsilon} + \dot{\beta} \tag{5}$$

where $\dot{F}$ is a material derivative of the deformation gradient tensor, L^e and L^p are the elastic and plastic parts of the velocity gradient tensor, $\dot{\varepsilon}$ is a strain rate that is the symmetric part of the L tensor and $\dot{\beta}$ is the spin tensor – the antisymmetric part of the velocity gradient one, respectively. For the ECAP process considered here and for the model in which the shear occurs in an inner core, the velocity gradient tensor along the intersection plane of two channels, expressed in the global (L) and in the local (L') coordinate systems is as follows (Eq. 6):

$$L = \frac{\dot{\gamma}}{2} \begin{bmatrix} 1 & -1 & 0 \\ 1 & -1 & 0 \\ 0 & 0 & 0 \end{bmatrix}, \quad L' = \begin{bmatrix} 0 & -\dot{\gamma} & 0 \\ 0 & 0 & 0 \\ 0 & 0 & 0 \end{bmatrix} \tag{6}$$

where $\dot{\gamma}$ is the shear rate ($\dot{\gamma} > 0$). Contrary to other SPD processes, all components of the velocity gradient tensor are known in the ECAP method. Based on the matrixes above, the symmetric and antisymmetric parts of the L tensor in the global coordinate system can be expressed (Eq. 7):

$$\dot{\varepsilon} = \frac{\dot{\gamma}}{2} \begin{bmatrix} 1 & 0 & 0 \\ 0 & -1 & 0 \\ 0 & 0 & 0 \end{bmatrix}, \quad \dot{\beta} = \frac{\dot{\gamma}}{2} \begin{bmatrix} 0 & -1 & 0 \\ 1 & 0 & 0 \\ 0 & 0 & 0 \end{bmatrix} \tag{7}$$

The $\dot{\varepsilon}$ tensor shows that the deformation state in the ECAP is the tension in the x direction and the compression in the y one. The spin tensor also indicates the rigid body rotation.

The dislocation slip is considered here as a main mechanism of a plastic deformation of the polycrystalline material. The slip is anisotropic and occurs only in selected slip planes determined

by the normal to this plane (n_α) and in selected slip directions described by the m_α vector lying on the slip plane [32]. The combination of n^α and m^α orthogonal each other vectors determines the slip systems. The twelve slip systems (M^α) defined by four octahedral planes {111} and three directions <110> are for the face-centered cubic (FCC or A1) structure considered here [33].

The slip does not change the orientation of a crystalline structure and the plastic strain is a result of a shear posed by the shearing stress – resolved shear stress (τ^α) (Eq. 8). According to the Schmid law, the slip occurs when shear stresses on the slip plane and in the slip direction reach the critical value – the critical resolved shear stress (τ^c) [34]. The plasticity criterion depending on the current stress state and the current crystal orientation is the following, therefore (Eq. 9) [35].

$$\tau^s = M^\alpha : \sigma \tag{8}$$

$$\tau^s - \tau^c = 0 \tag{9}$$

where σ is the Cauchy stress tensor and M^α is the Schmid orientation one defined as (Eq. 10):

$$M^\alpha = n^\alpha \otimes m^\alpha \tag{10}$$

There is not any relationship between the resolved shear stress and the slip rate $\dot{\gamma}$. Only the one value of the τ^c occurs for a plasticity.

The CP theory connects problems in different scales – i.e. macro- and micro- or nano- ones. The plastic part of the velocity gradient tensor L^p is expressed by the slip rate $\dot{\gamma}^\alpha$ of the α slip system (Eq. 11).

$$L^p = \sum_{i=1}^{N} \dot{\gamma}^\alpha \cdot M^\alpha = \sum_{i=1}^{N} \dot{\gamma}^\alpha \cdot n^\alpha \otimes m^\alpha \tag{11}$$

where N is the total number of slip systems.

Assuming the connection between different scales, the plastic strain rate $\dot{\varepsilon}^p$ and the plastic spin $\dot{\beta}^p$ tensors might be written (Eq. 12-13):

$$\dot{\varepsilon}^p = \frac{1}{2}\left(L^p + L^{pT}\right) = \sum_{\alpha=1}^{n} p^\alpha \cdot \dot{\gamma}^\alpha \tag{12}$$

$$\dot{\beta}^p = \frac{1}{2}\left(L^p - L^{pT}\right) = \sum_{\alpha=1}^{n} \omega^\alpha \cdot \dot{\gamma}^\alpha \tag{13}$$

where p^α and ω^α are symmetric and antisymmetric tensors defined by the Schmid tensor on selected α slip system, L^p is the plastic velocity gradient tensor.

In numerical simulations of the ECAP process here using the CP approach, the strain hardening of the polycrystalline material is assumed. According to Dawson et al. [36], the shear rate for $\dot{\gamma}^\alpha$ slip system evaluates as follows (Eq. 14):

$$\dot{\gamma}^\alpha = \dot{\gamma}_0 \left(\frac{|\tau^\alpha|}{g^\alpha}\right)^k \text{sgn}\left(\tau^\alpha\right) \tag{14}$$

where $\dot{\gamma}_0$ is a reference shear strain rate on the α slip system, τ^α is a resolved shear stress on the α slip system, k is the rate sensitivity

1652

coefficient and g^α is the critical shear stress on the α activated slip system to govern the isotropic hardening of the crystal. Assuming the kinematic hardening and the backstress associated with it, the shear rate might be rewritten as (Eq. 15) [37]:

$$\dot{\gamma}^\alpha = \dot{\gamma}_0 \, \text{sgn}\left(\tau^\alpha - x^\alpha\right)\left(\frac{\left|\tau^\alpha - x^\alpha\right|}{g^\alpha}\right)^k \qquad (15)$$

where x^α is a backstress which characterizes the nonlinear kinematic (directional) hardening of the crystal on the α slip system, g^α is the slip system strength and sgn is a signum function. The evolution of the backstress and the slip system strength ($\dot{g}^\alpha$) are as follows (Eq. 16-17):

$$x = a\dot{\gamma}^\alpha - c\left[1 - e_1\left(1 - \exp\left(-e_2\gamma\right)\right)\right]x^\alpha \left|\dot{\gamma}^\alpha\right| - dx^\alpha \qquad (16)$$

$$\dot{g}^\alpha = \sum_\beta h^{\alpha\beta} \dot{\gamma}^\beta \qquad (17)$$

where a is the initial hardening modulus of a slip system, c is the nonlinear hardening parameter, e_1 and e_2 describe the cyclic hardening saturation, $h^{\alpha\beta}$ is a hardening modulus defining the variation of slip resistance for the α slip system due to the slip rate on β slip system and might be defined as a relationship assuming both hardening and recovery (Eq. 18):

$$h^{\alpha\beta} = \begin{cases} h_0^\beta\left[1 - \dfrac{g^\beta}{g_s^\beta}\right]^{\alpha^\beta} & \text{for } \alpha = \beta \\[3mm] h_0^\beta q\left[1 - \dfrac{g^\beta}{g_s^\beta}\right]^{\alpha^\beta} & \text{for } \alpha \neq \beta \end{cases} \qquad (18)$$

where q is a latent hardening ratio, h_0^β is a hardening parameter for β slip system, g_s^β defines the slip resistance at hardening saturation for β slip system, and α^β is a material constant for β slip system defining the sensitivity of the hardening moduli to the slip resistance. It is assumed that $h^{\alpha\beta}$ is a self-hardening modulus for $\alpha = \beta$ or for $\alpha \neq \beta$, $h^{\alpha\beta}$ is a latent hardening one. In the FEPX software applied here, the latent hardening is assumed.

3. Numerical simulations of the ECAP process

The numerical calculations of the ECAP process were performed at two stages. Firstly, the macroscopic analysis in the commercial FEM program (ABAQUS) using the UMAT user-material procedure was done. The geometry of the model used in the macroscopic calculations is shown in Fig. 3. Details of the model are also contained in TABLE 1.

The macroscopic analysis of the ECAP process was done for the elastic-plastic material with a nonlinear isotropic hardening. Both Eulerian and Lagrangian approaches were tested and results for the pure Lagrangian approach are shown in this paper. Due to the application of relatively small corner radius in the analysis, the remeshing is not needed. The use of a counter
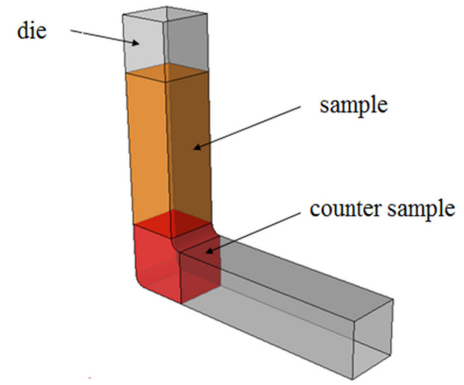

Fig. 3. The geometry of the model used in the macroscopic analysis

TABLE 1

Details of the model used in the macroscopic analysis

Parameter	Value
Numerical model	3-D
Material model	elastic-plastic
Integration procedure	implicit
Friction formulation	Coulomb friction
Friction coefficient	0.1
Element type	eight-node brick elements (C3D8)
Number of elements	29147
Number of nodes	31940

sample can also perform the analysis without the remeshing. The friction was also included and the Coulomb friction model with 0.1 friction coefficient was applied in numerical calculations.

The displacements obtained in the macroscopic FEM analysis are the kinematic input for the polycrystalline structure. The microscopic analysis using the CP approach is done in NEPER and FEPX open software which can include, e.g. slip systems, hardening and anisotropy of grains in calculations [38]. Due to the large size of a task, the calculations were done only for a point near the core of a sample, which is represented by the representative volume element (RVE) (Fig. 4).
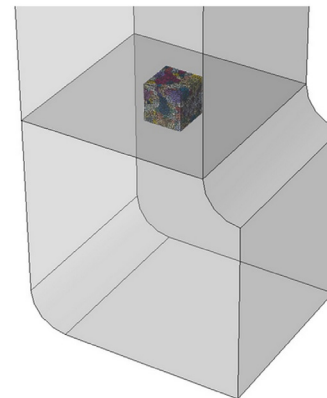

Fig. 4. The CPFEM simulation of the ECAP process used here

The numerical analyses are done for a RVE with both 400 and 800 randomly oriented grains (Fig. 5). The calculations

are performed for a generic C11000 copper alloy modeled as a polycrystalline material with the FCC structure and with 12 slip systems. The elastic and plastic parameters for the material available in the literature [38] are contained in TABLE 2. The displacement-controlled analysis was considered here on the microscopic level.
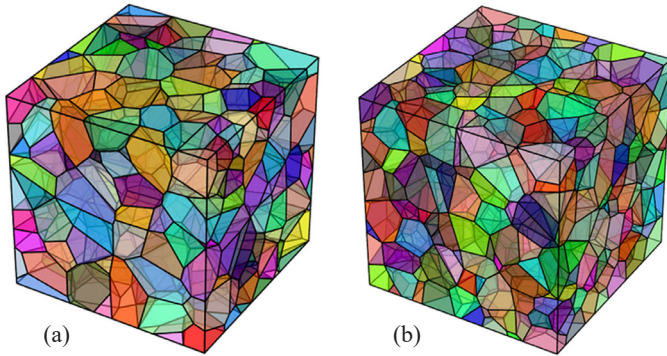

(a)　　　　　　　　　　(b)

Fig. 5. The RVE with 400 (a) and 800 (b) grains

TABLE 2

Elastic and plastic parameters of the copper used in the CP analysis

Elastic arameters	
Young modulus E [MPa]	1.66×10^5
Poisson's ratio v [-]	0.33
Elastic constant C_{11} [MPa]	245×10^3
Elastic constant C_{21} [MPa]	155×10^3
Elastic constant C_{44} [MPa]	62.5×10^3
Plastic parameters	
Material constant m [-]	0.05
Reference shear strain rate $\dot{\gamma}_0$ [s^{-1}]	1.0
Fixed-state hardening rate scaling coefficient h_0 [MPa]	200.0
Initial slip system strength g_0 [MPa]	210.0
Initial slip system saturation strength g_{s0} [MPa]	330.0
Rate sensitivity coefficient k [-]	1.0

The numerical calculations were done iteratively in a loop using equations presented in section 2 for a lot of computational steps which is shown in Fig. 6. The implicit integration procedure was tested here.
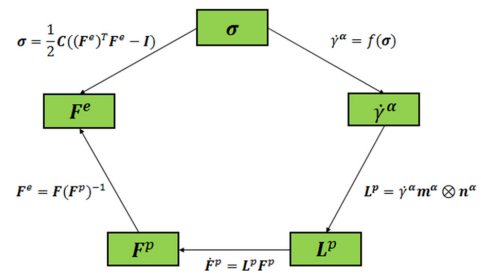

Fig. 6. The loop showing calculations using the crystal plasticity theory

4. Results and discussion

At the first stage, the macroscopic analysis of the ECAP process for a copper alloy was done using the commercial FEM software. The von Misses stress distribution in the sample is shown in Fig. 7. The highest stress values were noted near the corners of the die.
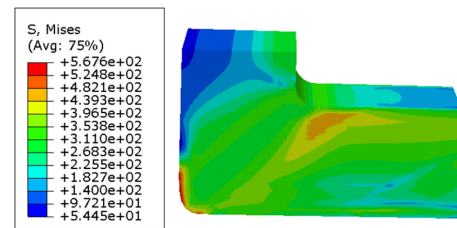

Fig. 7. The Mises stress distribution in the copper sample during the ECAP process

Fig. 8 presents the distribution of the effective plastic strain (PEEQ) in the deformed sample. The plastic deformation zone
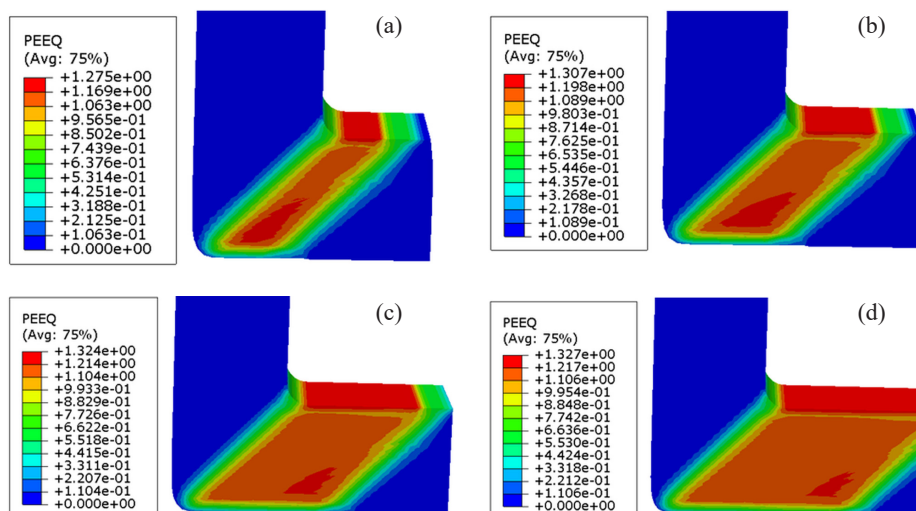

Fig. 8. The PEEQ distribution in the copper sample during the ECAP process; step time 0.23 s (a); step time 0.33 s (b) step time 0.47 s (c); step time 0.67 s (d)

1654

starts from the die corners after passing through the shearing plane and spreads during the process. The highest plastic strains are in the middle part of the plastic deformation zone and decrease outside the one.
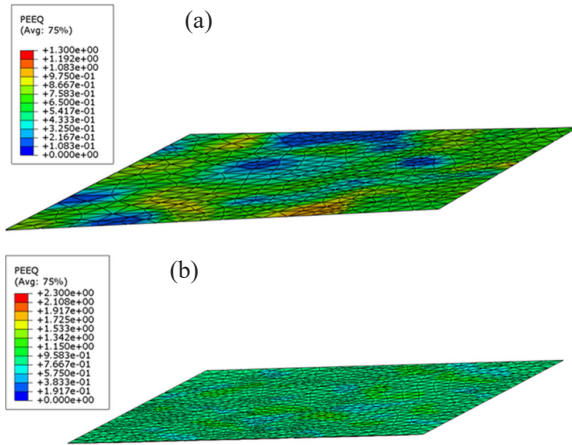

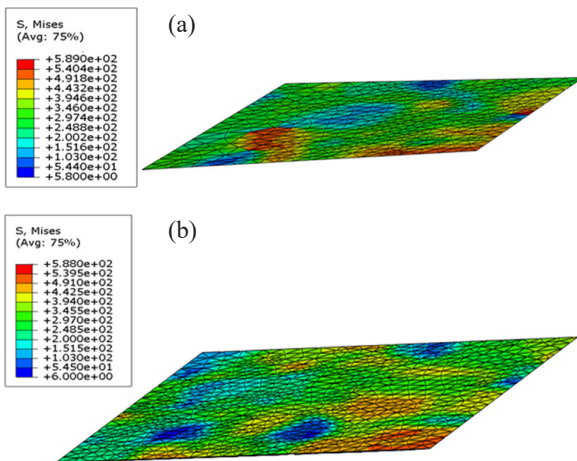Fig. 9. The PEEQ distribution in the copper sample for 400 (a) and 800 (b) grains

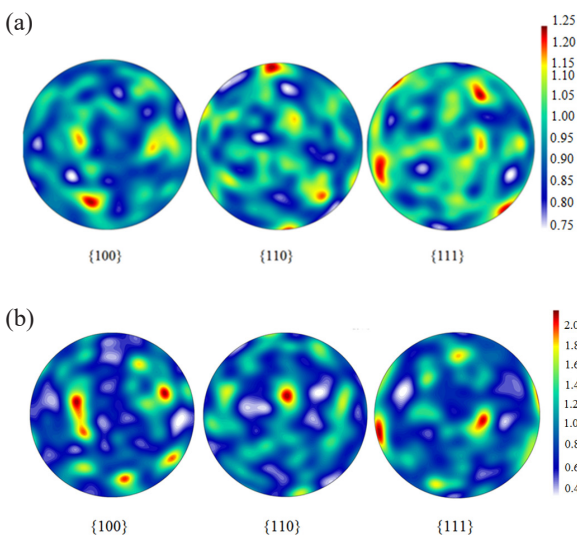Fig. 10. The Misses stress distribution in the copper sample for 400 (a) and 800 (b) grains

Fig. 11. Pole figures before (a) and after (b) the ECAP process

Using the displacements obtained in the macroscopic analysis, the microstructural calculations on the basis of the CP approach were done. The stress and plastic strain distributions in a RVE both for 400 and 800 grains after the ECAP are presented in Figs. 9 and 10. The heterogeneous distribution of stress and plastic strain inside the sample is noted. Some grains were characterized by higher stress and plastic strain values which is a result of different crystal orientations in grains. The results obtained in the analysis on the basis of the CP theory are compatible with the macroscopic analyses, as well as, with theoretical predictions [39-40].

In order to examine the texture evolution, the pole figures showing the texture before and after the ECAP process with one pass for a copper alloy with FCC structure were compared. The {100}, {110} and {111} pole figures are shown in Fig. 11.

5. Summary and conclusions

In this paper, the application of the use of the crystal plasticity (CP) theory in numerical calculations of the equal-channel angular pressing (ECAP) is presented. At the first step, the macroscopic simulations of the ECAP were done using the commercial FEM solver. The displacements obtained in the macroscopic calculations are used later on as the kinematic input for the polycrystalline structure in the microscopic analyses. The stress and equivalent plastic strain distributions, as well as, pole figures before and after the ECAP were obtained. The heterogeneity of stress and plastic strain within grains was noted. On the basis of results obtained, the main conclusions are as follows:

1. The different orientations of crystals in grains result in the heterogeneous distribution of stress and strain within the material. The results obtained for both macroscopic and microscopic analyses are coincident.

2. The complex state of stress and strain is noted in the sample extruded near the walls. The shear and the rotation are in the inner core of a sample extruded.

3. The results obtained in numerical analyses using the CP theory here are consistent with theoretical solutions available in literature.

4. The CP theory gives more detailed information about phenomena occurring in materials which are deformed plastically during the materials forming processes, e.g. in SPD processes. However, the numerical calculations on the microscale level are associated with the writing of a user material procedure which is a very time-consuming and difficult task.

5. Due to the large size of the task considered, the calculations on the CP level are done for only a point represented by the representative volume element (RVE). The analysis for the whole sample on the microscopic level results in very long time of calculations.

The results presented here show the potential of the application of the CP approach in simulations of the ECAP in order to optimize the process also in the industrial applications and give

the fulfill description of phenomena occurring in the material. In further research, the numerical simulations of the ECAP process using other CP models, including viscoplastic ones will be done. The other plastic deformation mechanisms, i.e. twinning will be also included. The numerical calculations for dynamic analyses are also planned in the future.

REFERENCES

[1] M. Wójcik, A. Skrzat, Contin. Mech. Thermodyn. **32**, 959-969 (2020). DOI: https://doi.org/10.1007/s00161-019-00805-y

[2] K. Kowalczyk-Gajewska, S. Stupkiewicz, Arch. Metall. Mater. **58** (1), 113-118 (2013). DOI: https://doi.org/0.2478/v10172-012-0160-y

[3] P. Wei, C. Lu, K.Tieu, G.Y. Deng, IOP Conf. Ser.: Mater. Sci. Eng. **63** (1), 012045 (2014). DOI: https://doi.org/10.1088/1757-899X/63/1/012045

[4] K.B. Golafshani, S. Nourouzi, H.J. Aval, Mater. Sci. Technol. **35** (9), 1061-1070 (2019). DOI: https://doi.org/10.1080/02670836.2019.1612577

[5] D.N. Lee, Scr. Mater. **43** (2), 115-118 (2000). DOI: https://doi.org/10.1016/S1359-6462(00)00377-8

[6] L. Cui, S. Shao, H. Wang, G. Zhang, Z. Zhao, C. Zhao, Processes **10**, 2181 (2022). DOI: https://doi.org/10.3390/pr10112181

[7] E. Baysal, O. Koçar, E. Kocaman, U. Köklü, Metals **12**, 1800 (2022). DOI: https://doi.org/10.3390/met12111800

[8] M.H. Shaeri, M. Shaeri, M. Ebrahimi, M.T. Salehi, S.H. Seyyedein, Prog. Nat. Sci. **26** (2), 182-191 (2016). DOI: https://doi.org/10.1016/j.pnsc.2016.03.003

[9] G.M. Naik, S. Narendranath, S.S. Satheesh Kumar, J. Mater. Eng. Perform **28**, 2610-2619 (2019). DOI: https://doi.org/10.1088/2053-1591/ab2ddf

[10] M.I. Abd El Aal, M.M. Sadawy, Trans. Nonferrous Met. Soc. China **25** (12), 3865-3876 (2015). DOI: https://doi.org/10.1016/S1003-6326(15)64034-1

[11] D. Lu, J. Jiang, X. Liao, K.M. Nesterov, R.K. Islamgaliev, R.Z. Valiev, K. Liu, J. Mater. Eng. Perform **26**, 2110-2117 (2017). DOI: https://doi.org/10.1007/s11665-017-2660-4

[12] R. Kočiško, T. Kvačkaj, A. Kováčová, J. Achiev. Mater. Manuf. Eng. **62** (1), 25-30 (2014). DOI: https://doi.org/10.12693/APhysPolA.131.1336

[13] M. El-Shenawy, M.M.Z. Ahmed, A. Nassef, M. El-Hadek, B. Alzahrani, Y. Zedan, W.H. El-Garaihy, Metals **11**, 938 (2021). DOI: https://doi.org/10.3390/met11060938

[14] A.I. Alateyah, M.M.Z. Ahmed, Y. Zedan, H.A. El-Hafez, M.O. Alawad, W.H. El-Garaihy, Experimental and Numerical Investigation of the ECAP Processed Copper: Microstructural Evolution, Crystallographic Texture and Hardness Homogeneity, Metals **11**, 607 (2021). DOI: https://doi.org/10.3390/met11040607

[15] S. Li, Acta Materialia **56** (5), 1031-1043 (2008). DOI: https://doi.org/10.1016/j.actamat.2007.11.003

[16] S. Ferrasse, V.M. Segal, S.R. Kalidindi, F. Alford, Mater. Sci. Eng. A **368** (1-2), 28-40 (2004). DOI: https://doi.org/10.1016/j.msea.2003.09.077

[17] G. Yang, S.J. Park, Materials **12**, 2003 (2019). DOI: https://doi.org/10.3390/ma12071177

[18] G. Deng, PhD thesis, Crystal plasticity finite element method simulation of equal channel angular pressing, University of Wollongong, Wollongong, Australia (2014).

[19] M.P. Petkov, E. Elmukashfi, E. Tarleton, A.C.F. Cocks, IJMS **211**, 106715 (2021). DOI: https://doi.org/10.1080/14786435.2022.2121867

[20] S. Li, I.J. Beyerlein, D.J. Alexander, S.C. Vogel, Acta Mater. **53** (7), 2111-2125 (2005). DOI: https://doi.org/10.1016/j.actamat.2005.01.023

[21] L.S. Tóth, R.A. Massion, L. Germain, S.C. Baik, S. Suwas, Acta Mater. **52** (7), 1885-1898 (2004). DOI: https://doi.org/10.1016/j.actamat.2003.12.027

[22] E. Hosseini, M. Kazeminezhad, Comput. Mater. Sci. **44** (3), 962-967 (2009). DOI: https://doi.org/10.1016/j.commatsci.2008.07.002

[23] C.F. Gu, L.S. Tóth, C.H.J. Davies, Scr. Mater. **65** (2), 167-170 (2011). DOI: https://doi.org/10.1016/j.scriptamat.2011.04.009

[24] K. Kowalczyk-Gajewska, Arch. Mech. **61** (6), 475-503 (2009).

[25] H.R. Wenk, P.V. Houtte, Rep. Prog. Phys. **67**, 1367-1428 (2004). DOI: https://doi.org/10.1088/0034-4885/67/8/R02

[26] A. Ostapovets, P. Šedá, A. Jäger, P. Lejček, Bull. Russ. Acad. Sci. Phys. **76**, 76-79 (2012). DOI: https://doi.org/10.3103/S1062873812010224

[27] R.A. Lebensohn, C.N. Tomé, Acta Metall. Mater. **41** (9), 2611-2624 (1993). DOI: https://doi.org/10.1016/0956-7151(93)90130-K

[28] R. Kiryk, H. Petryk, Arch. Mech. **50** (2), 247-263 (1998).

[29] K. Kowalczyk-Gajewska, S. Stupkiewicz, H. Petryk, K. Frydrych, IOP Conf. Ser.: Mater. Sci. Eng. **63**, 012040 (2014). DOI: https://doi.org/10.1088/1757-899X/63/1/012040

[30] R.J. Asaro, Adv. Appl. Mech. **23**, 1-115 (1983). DOI: https://doi.org/10.1016/S0065-2156(08)70242-4

[31] R.J. Asaro, A. Needleman, Acta Metallurgica **33** (6), 923-953 (1985). DOI: https://doi.org/10.1016/0001-6160(85)90188-9

[32] K. Frydrych, K. Kowalczyk-Gajewska, Mater. Sci. Eng. A **658**, 490-502 (2016). DOI: https://doi.org/10.1016/j.msea.2016.01.101

[33] K. Frydrych, Eng. Trans. **69** (4), 337-352 (2021). DOI: https://doi.org/10.24423/EngTrans.1320.20210908

[34] H. Petryk, M. Kursa, Arch. Mech. **63** (3), 287-310 (2011).

[35] W. Wajda, Ł. Madej, H. Paul, Arch. Metall. Mater. **58** (2), 493-496 (2013). DOI: https://doi.org/10.2478/amm-2013-0024

[36] P.R. Dawson, D.E. Boyce, J.S. Park, E. Wielewski, M.P. Miller, Acta Mater. **144**, 92-106 (2018). DOI: https://doi.org/10.1016/j.actamat.2017.10.032

[37] M. Wójcik, A. Skrzat, ASTRJ **16** (5), 163-177 (2022). DOI: https://doi.org/10.12913/22998624/154025

[38] https://fepx.info/doc/examples.html, accessed: 22.12.2022

[39] F. Roters, P. Eisenlohr, L. Hantcherli, D.D. Tjahjanto, T.R. Bieler, D. Raabe, Acta Mater. **58** (4), 1152-1211 (2010). DOI: https://doi.org/10.1016/j.actamat.2009.10.05

[40] V.M. Segal, Mater. Sci. Engng. A **197**, 157-164 (1995). DOI: https://doi.org/10.1016/0921-5093(95)09705-8